ChemComm

COMMUNICATION

Insights into the Electrochemical Performances of Bi Anodes for Mg Ion Batteries Using ^{25}Mg Solid State NMR Spectroscopy

Received 00th January 20xx,
Accepted 00th January 20xx

DOI: 10.1039/x0xx00000x

www.rsc.org/chemcomm

Zigeng Liu[a], Jeongjae Lee[a], Guolei Xiang[a], Hugh F. J. Glass[a,b], Evan N. Keyzer[a], Siân E. Dutton[b], and Clare P. Grey[a]*

Bi nanowires as anode materials for Mg ion batteries exhibit excellent electrochemical behaviour forming Mg_3Bi_2; this is in part ascribed to the rapid Mg mobility between the two Mg sites of Mg_3Bi_2, as revealed by the ^{25}Mg NMR spectra of Mg_3Bi_2 formed electrochemically and *via* ball-milling. A mechanism involving hops into vacant Mg sites is proposed.

Lithium ion batteries (LIBs) are currently dominating the portable electronic devices power supply market and have been integrated into electric vehicles (EVs). Cost and supply restrictions will become important issues for LIBs due to the limited and unevenly distributed lithium resources particularly as the EV and grid storage markets grow. Recently, batteries with multivalent ions such as Mg^{2+} and Al^{3+} have drawn considerable interest as potential replacements to LIBs particularly in applications where high volumetric energy density is important.[1,2] In particular, Mg ion batteries (MIBs) are attractive alternatives due to the negative reduction potential of Mg (-2.37 V *vs.* SHE), the abundance of Mg in the earth's crust and the large volumetric capacity of Mg (3832 mAh/cm^3). However, there are at least three major factors hindering the application of MIBs. First, most of the electrolytes cannot survive at high voltage (>3.5 V), limiting the operating voltage of the cathode materials and the energy density of MIBs. Second, the sluggish diffusion of Mg ions in electrode materials hampers the rate capacity of MIBs. Third, the reaction of electrolytes with Mg metal leads to an insulating passivation layer which restricts electron and Mg ion transport and increases overpotential, eventually completely preventing Mg plating and stripping.[3–6] While electrolytes that allow reversible stripping and plating of Mg have been identified,[3–5] they are not compatible with high voltage cathode materials. To circumvent these limitations, new electrolytes and electrode materials have been investigated. In particular, use of an alternative anode material to Mg metal may bypass the issue of the passivation layer and enable the use of other higher voltage electrolytes. To this end, recent reports have demonstrated that Bi metal, which has a theoretical capacity of 385 mAh/g and a very low discharge plateau of 0.2 V *vs.* Mg, is compatible with different electrolytes and counter electrodes.[7–12] Bi incorporates Mg through an alloying reaction to form Mg_3Bi_2. However, a volume expansion of 95.3 % is observed when Bi is fully converted to Mg_3Bi_2, which is one of the reasons for the observed capacity fade on cycling Bi.[7] To mitigate this issue, different morphologies, such as nanotubes, have been used to improve the long-term cycling life of Bi electrodes.[9] Ball milled Mg_3Bi_2 also demonstrates electrochemical reactivity when used as a Mg source for a MIB system.[10]

The behaviour of Bi electrode throughout the cycling process was previously investigated through X-ray diffraction techniques.[7,9–11] Although these studies provide valuable insights into the correlations between the long-range bulk structural changes and the electrochemical properties of Bi electrodes, they provide little information on the local structures and dynamics of Mg ions. Thus, we have investigated a Bi electrode comprised of Bi nanowires employing ^{25}Mg solid-state nuclear magnetic resonance (ssNMR) spectroscopy to gain more insights into the magnesiation and demagnesiation processes. Information about the Mg ion dynamics in Mg_3Bi_2 was obtained through a variable temperature (VT) ^{25}Mg NMR study on samples prepared *via* electrochemical and mechanical methods.

Bi nanowires were prepared by reduction of aqueous $BiCl_3$ with Zn (see SI for further details).[13] The TEM image (Figure 1) shows that the sample comprises individual nanowires with diameters of ~40 nm and lengths of ~300 nm.

Figure 2a shows the galvanostatic curve obtained for Bi nanowires when used as a MIB anode under a current density 192.5 mA/g,

[a] Department of Chemistry, University of Cambridge, Cambridge, CB2 1EW, UK. E-mail: cpg27@cam.ac.uk;
[b] Cavendish Laboratory, University of Cambridge, Cambridge, CB3 0HE, UK.
Electronic Supplementary Information (ESI) available: Experimental details and supporting figures. See DOI: 10.1039/x0xx00000x

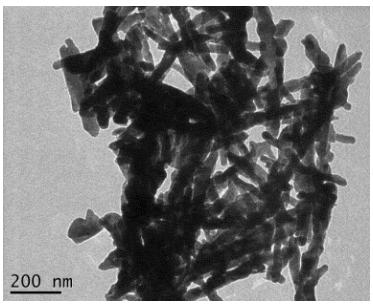

Fig. 1 TEM image of Bi nanowires, taken at 200 kV.

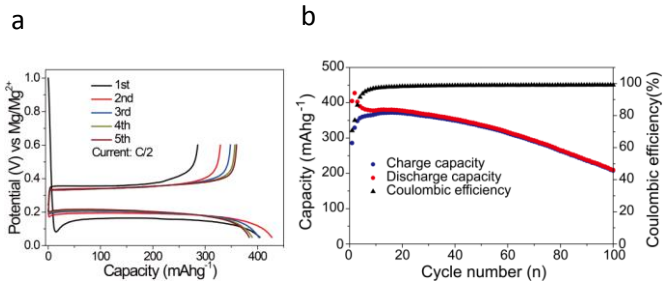

Fig. 2 (a) The first five electrochemical profiles of a Bi/Mg cell at a rate of C/2 with a Grignard electrolyte. (b) Discharge-charge performances of Bi anode at a C/2 rate and the coulombic efficiency.

corresponding to a rate of C/2. The reversible capacity drops to > 50 % of the theoretical capacity (207 mAh/g) after 100 cycles (Figure 2b) at a C/2 rate. The coulombic efficiency is close to 100% after 10 cycles and is very stable in the subsequent cycling. The high cycling stability and stable coulombic efficiency indicate that Bi nanowires are good anodes for MIB systems.

^{25}Mg ssNMR was employed to study the magnesiation of the Bi electrode in more detail. ^{25}Mg NMR, however, is quite challenging because of the low (10 %) natural abundance of the only NMR active Mg isotope (^{25}Mg), a very low gyromagnetic ratio (2.606 MHz/T) and a large quadrupolar moment (I=5/2, Q=0.2 barns), leading to low receptivity, long measurement times, and broad resonances. Despite these difficulties, we have successfully obtained high resolution ^{25}Mg NMR spectra of Bi anodes along the discharge-charge curve (Figure 3). In figure 3a, only a single resonance at -97 ppm is observed, whose intensity increases following the magnesiation process of Bi anode until it reaches its maximum at the end of discharge and disappears at the end of charge. The fact that only a single ^{25}Mg resonance is seen at the same position for all samples suggests that this resonance should be assigned to Mg_3Bi_2, and the intensity evolution of this resonance reflects a two-phase alloying reaction of Mg and Bi, in agreement with XRD results in previous

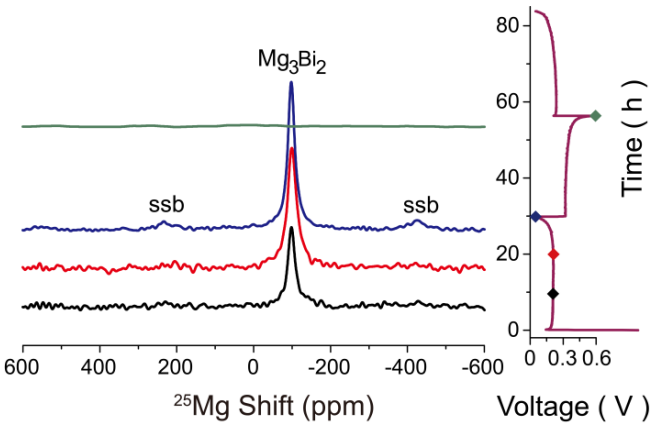

Fig. 3 (a) Quantitative ^{25}Mg NMR spectra of Bi anode at various states of charge (with colour corresponding to the points shown on the electrochemistry profile in (b)) at a spinning rate of 14 kHz. Spinning sidebands labeled in the spectra as ssb. (b) The corresponding electrochemical profile of Bi anode cycled at a current density of 12.8 mA/g.

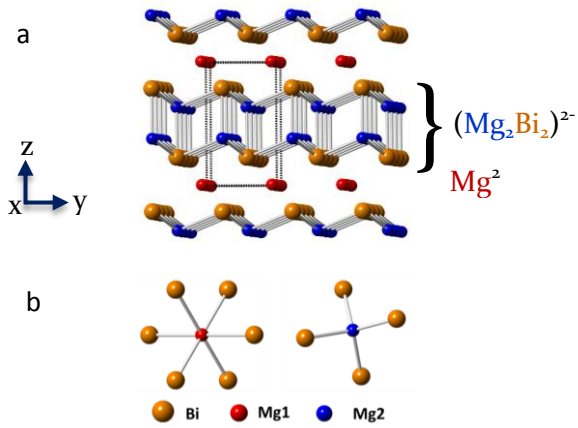

Fig. 4 (a) Schematic structure of Mg_3Bi_2. (b) Local environments of the Mg1 and Mg2 sites.

reports.[7,9,11] No evidence for MgO is seen, which gives rise to a distinctive sharp resonance at 26 ppm.

Mg_3Bi_2 is a Zintl compound with an anti-La_2O_3 structure (space group $P\bar{3}m1$) that contains two crystallographically distinct Mg sites (Figure 4), which we denote as Mg1 and Mg2, with site multiplicities of 1:2.[7,15] The structure is formed of alternating layers of Mg^{2+} cations (Mg1) and covalent $(Mg_2Bi_2)^{2-}$ anionic bi-layers (Mg2), where the Mg1 (1a) and Mg2 (2d) sites are octahedrally and tetrahedrally coordinated by Bi, respectively (Figure 4b). Thus two distinct resonances should be seen in the ^{25}Mg NMR spectra of Mg_3Bi_2, with an intensity ratio of 1:2. On the basis of previous studies which reported high rate (5 C) performances for Bi nanotubes,[9] we suggest that Mg_3Bi_2 may display fast Mg ion transport. Furthermore, Mg_3Bi_2 displays fast ionic conduction above a phase transition at 703 °C.[16] Our NMR results suggest that the Mg mobility is sufficiently fast even at room temperatures to result in averaging of the individual NMR

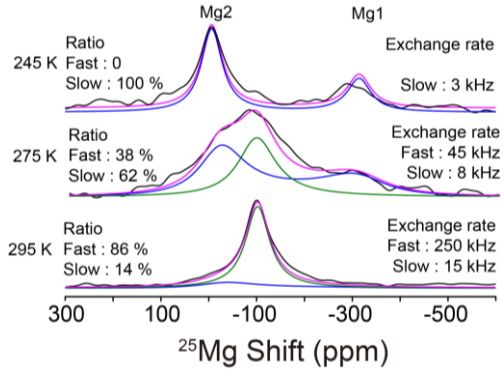

Fig. 5 ^{25}Mg VT NMR spectra of the electrochemically prepared Mg_3Bi_2 acquired at a spinning rate of 20 kHz. The experimental spectra (black lines) were fit (pink lines) with a model with two different correlation times for two-site exchange: fast (green lines) and slow (blue lines). The spectra have been scaled so that their heights are equal. The estimated errors for the slow and fast exchange rates are ±1 kHz and ±10 kHz, respectively.

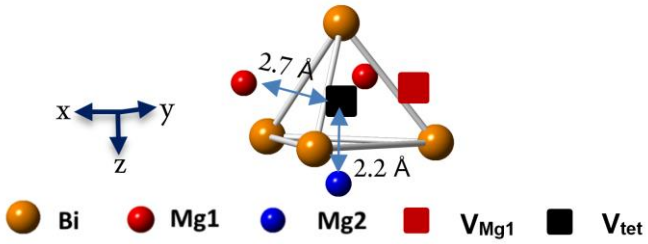

Fig. 6 Schematic structure of Mg_3Bi_2 with V_{oct} (red square) and V_{tet} (black square).

signals to yield a single resonance. To test this hypothesis, VT NMR experiments at low temperature were performed in order to reduce the mobility of the Mg ions.

^{25}Mg NMR spectra of electrochemically prepared Mg_3Bi_2 at different temperatures are shown in Figure 5a. The intensity of the resonance at -97
ppm starts to decrease and two new resonances at -6 ppm and -306 ppm appear when the temperature is reduced from 295 to 275 K. At 245 K only the two new resonances are observed with a relative intensity ratio of approximately 2:1 (Figure 5), which are assigned to Mg2 (-6 ppm) and Mg1 (-306 ppm), respectively, based on this relative intensity. Rapid Mg ion hopping between these two sites should, therefore, result in a coalescence of these two resonances into a single resonance at the average shift weighted by the site occupancy of the Mg1 and Mg2 sites (-106 ppm); this is close to the shift observed experimentally at 295 K of -97 ppm, confirming that both Mg ions are involved in the motional process. Upon coalescence, the exchange frequency, k_{ex},[17] should be equal to or greater than 28.5 kHz ($k_{ex} = \pi v/\sqrt{2} = 28.5$ kHz; v is the separation between the two resonances), corresponding to a correlation time, τ_c,[17] of 35 µs ($\tau_c = 1/k_{ex} = 3.5\times10^{-5}$ s). However, the line shape (particularly of the 275 K spectrum, where the resonance at -97 ppm is observed in addition to the resonances at -6 and -306 ppm) is not consistent with a simple two-site exchange process, but results from a distribution of correlation times for motion within the sample. Line shape simulation were, therefore, performed with the simplest model possible, and one that was shown previously to describe (fluoride) ion conduction in samples with non-uniform concentrations of defects (anion vacancies) in the sample.[18] Two subsets of spins, a more rigid component, likely further away from defects in the Mg_3Bi_2 sample, and a more mobile component nearer the defects, are used to describe the system. The relative population of the two components are allowed to vary with temperature. At low temperatures all the Mg^{2+} ions are in the slow regime, while 60 % of the ions have entered the fast regime (*i.e.*, undergo hops between the two sites with a frequency >28.5 kHz) at 275 K. At 295 K, approximately 86 % of the ions are in the fast regime. This change in relative population of the fast and slow moving ions is characteristic of a distribution of correlation times, where an increasingly higher fraction of ions enters the intermediate and then the fast regime of motion as the temperature is increased.[18] Much higher quality data would be required to analyse the width and nature of the distribution of correlation times.

Seebeck coefficient measurements have shown that Mg_3Bi_2 is a *p*-type semiconductor, suggesting that electron holes are present in the valence band.[19] Thus, we tentatively suggest that Mg^{2+} vacancies are present in the Mg^{2+} (Mg1) layers at low temperatures, compensated by electron holes in the more covalent $(Mg_2Bi_2)^{2-}$ layers. Hopping of Mg^{2+} ions into the vacant

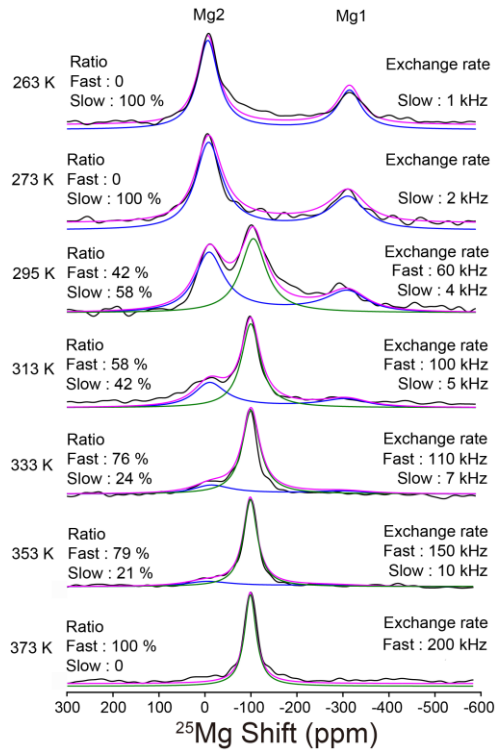

Fig. 7 ^{25}Mg VT NMR spectra of Mg_3Bi_2 synthesised by mechanical alloying, measured at a spinning rate of 14 kHz. The experimental spectra (black lines) were fit (pink lines) with a model with fast (green lines) and slowly exchanging sites (blue lines). The spectra have been scaled so that their heights are

equal. The estimated error bar for the slow and fast exchange rates are ±1 kHz and ±10 kHz, respectively.

Mg1 sites will result in Mg^{2+} transport. One possible explanation for the difference between the weighted average of the Mg1 and Mg2 resonances (-106 ppm) and the experimentally observed value (-97 ppm) is that it reflects a smaller relative population of the Mg1 ions (resonating at -306 ppm) than expected based on the crystal structure. Assuming the Mg2 sites are fully occupied, a site occupancy of 91 % is obtained for the Mg1 sites. While this lower site occupancy is consistent with our proposed defect model, the value must only be taken as a rough estimate; we have not, for example, taken into account the effect that electron holes have on the NMR shifts.

A close examination of the structure (Figure 4) reveals that Mg1 – Mg1 hops must occur *via* empty tetrahedral sites, V_{tet}, in the Mg1 layers (Figure 6). The Bi_4 tetrahedra enclosing these vacant sites share faces with the Mg2 tetrahedral sites. Thus a Mg1 – Mg1 hop will involve passing through an interstitial site (V_{tet}) (Figure 6) with a long Mg – Mg contact (of approximately 2.7 Å), resulting in a large activation energy. In contrast, since the Mg2 sites are tetrahedrally coordinated, the V_{tet} – Mg2 distance is shorter (approximately 2.2 Å). Thus, a hop of a Mg2 ion *via* V_{tet} into an empty Mg1 site should be associated with a lower activation barrier, favouring a mechanism involving Mg1 – Mg2 hops. Calculations are in progress to explore the transport mechanisms in greater detail.

In order to explore the dynamics further and improve the signal-to-noise ratio of the spectra, we investigated a larger volume Mg_3Bi_2 sample, synthesised by high-energy ball milling of Bi and Mg powders (structural refinement from synchrotron XRD in Figure S2b). 10.5(5) wt % of Bi is observed in thissample even when an excess of 33.3 wt % of Mg is used to compensate the Mg loss during ball-milling. The ^{25}Mg NMR spectrum of this material (Figure 7) at 263 K contains two well-resolved peaks at -8 ppm (Mg2) and -315 ppm (Mg1), close to those (within the experimental error) found for the electrochemically prepared Mg_3Bi_2 sample. The "coalescence" resonance at -96 ppm coexists with the Mg1 and Mg2 resonances at 295 K and accounts for 42 % of the total intensity. Intensities of the residual Mg1 and Mg2 resonances decreases as the temperature increases until 373 K, where only the coalescence resonance is left. The results are qualitatively consistent with the results from the electrochemically prepared sample. However, the ball-milled Mg_3Bi_2 sample shows a higher coalescence temperature than the electrochemically prepared Mg_3Bi_2 sample, indicating that the mobility of the Mg ions in the latter sample is higher. The difference in Mg-ion transport is most likely due to the presence of a higher concentration of defects in the Mg_3Bi_2 sample prepared electrochemically, presumably because it is formed at room temperature while the mechanical alloying process involves an increased temperature during high-energy ball milling. It is non-trivial to extract an activation barrier for Mg transport, due to the observed distribution of correlation times as discussed in more detail in the SI.

To conclude, we have synthesised Bi nanowires, *via* an aqueous route, which can cycle *vs*. Mg for multiple cycles with excellent coulombic efficiency. ^{25}Mg NMR spectra confirmed the two-phase reaction of Bi and Mg. Fast exchange between the two Mg sites inside the Mg_3Bi_2 structure was observed with ^{25}Mg VT NMR experiments and a hop mechanism involving Mg1 and Mg2 exchanging *via* an interstitial tetrahedral site is proposed. Our current work with Bi is focused on understanding the mechanism and pathway for the Mg diffusion and exploring the compatibility of Bi with a variety of Mg electrolytes for a full MIB system. The work has additional implications beyond the battery field because the mobility of Mg in this class of materials, and the possibility of altering this via appropriate doping, has implications for the Mg-based Zintl phases that have been proposed, or have been shown to be, good thermoelectric materials for power generation.

References

1 N. Amir, Y. Vestfrid, O. Chusid, Y. Gofer and D. Aurbach, *J. Power Sources*, 2007, **174**, 1234.

2 E. Levi, M. D. Levi, O. Chasid and D. Aurbach, *J. Electroceramics*, 2009, **22**, 13.

3 H. D. Yoo, I. Shterenberg, Y. Gofer, G. Gershinsky, N. Pour and D. Aurbach, *Energy Environ. Sci.*, 2013, **6**, 2265.

4 R. Mohtadi and F. Mizuno, *Beilstein J. Nanotechnol.*, 2014, 5, 1291.

5 J. Muldoon, C. B. Bucur and T. Gregory, *Chem. Rev.*, 2014, **114**, 11683.

6 M. S. Park, J. G. Kim, Y. J. Kim, N. S. Choi and J. S. Kim, *Isr. J. Chem.*, 2015, **55**, 570.

7 T. S. Arthur, N. Singh and M. Matsui, *Electrochem. Commun.*, 2012, **16**, 103.

8 M. Sedighi, B. Arghavani Nia, H. Zarringhalam and R. Moradian, *Eur. Phys. J. Appl. Phys.*, 2013, **61**, 10103.

9 Y. Shao, M. Gu, X. Li, Z. Nie, P. Zuo, G. Li, T. Liu, J. Xiao, Y. Cheng, C. Wang, J. G. Zhang and J. Liu, *Nano Lett.*, 2014, **14**, 255.

10 F. Murgia, L. Stievano, L. Monconduit and R. Berthelot, *J. Mater. Chem. A*, 2015, **3**, 16478.

11 A. Benmayza, M. Ramanathan, N. Singh, F. Mizuno and J. Prakash, *J. Electrochem. Soc.*, 2015, **162**, A1630.

12 M. Ramanathan, A. Benmayza, J. Prakash, N. Singh and F. Mizuno, *J. Electrochem. Soc.*, 2016, **163**, A477.

13 B. Yang, C. Li, H. Hu, X. Yang, Q. Li and Y. Qian, *Eur. J. Inorg. Chem.*, 2003, **20**, 3699.

14 R. A. DiLeo, Q. Zhang, A. C. Marschilok, K. J. Takeuchi and E. S. Takeuchi, *ECS Electrochem. Lett.*, 2014, **4**, A10.

15 A. A. Nayeb-Hashemi and J. B. Clark, *Bull. Alloy Phase Diagrams*, 1985, **6**, 528.

16 F. Zhang, Y. Tang, B. Hu, S. Liu, Y. Du and Y. Zhang, *J. Min. Metall. Sect. B Metall.*, 2014, **50**, 115.

17 A. Abragam, *The Principles of Nuclear Magnetism*, Oxford, Clarendon Press, 1961.

18 F. Wang and C. P. Grey, *J. Am. Chem. Soc.*, 1998, **120**, 970.

19 V. Ponnambalam and D. T. Morelli, *J. Electron. Mater.*, 2013, **42**, 1307.